

# Journal of Cleaner Production

## DSDMA: Dynamic Spray Drift Mitigation Algorithm for Optimal UAV Spraying in Agriculture

--Manuscript Draft--

<b>Manuscript Number:</b>	JCLEPRO-D-25-13064
<b>Article Type:</b>	Original article
<b>Keywords:</b>	Precision agriculture; Wind drift; Unmanned Aerial Vehicles; Spray optimization; Spray drift; Drone simulation.
<b>Corresponding Author:</b>	Rajni Goyal Sant Longowal Institute of Engineering and Technology INDIA
<b>First Author:</b>	Rajni Goyal
<b>Order of Authors:</b>	Rajni Goyal  Srinjoy Chakraborty  Amar Nath, PhD  Utkarsh Niranjan, PhD
<b>Abstract:</b>	Spray drift caused by wind remains a major challenge in UAV-based agricultural spraying, often resulting in off-target contamination, reduced application efficiency, and environmental pollution. To address this issue, this study proposes an aerodynamic-based framework to ensure precise and effective agrochemical deposition. Central to this framework is the Dynamic Spray Drift Mitigation Algorithm (DSDMA), which dynamically adjusts UAV waypoints in real time by incorporating wind parameters—such as speed, direction, and flow regimes (laminar, transitional and turbulent)—to proactively correct droplet displacement before it occurs. To stabilize the UAV's trajectory under varying wind conditions, a Proportional-Integral-Derivative (PID) controller is integrated into the system. This controller effectively compensates for positional errors caused by wind-induced drag forces, ensuring improved path tracking during spraying operations. The complete framework is validated in a high-fidelity simulation environment built on AirSim, ROS2, PX4, and Unreal Engine, offering realistic aerodynamic and flight dynamics. Simulation results demonstrate that DSDMA significantly reduces spray drift, as measured by the Mean Absolute Error (MAE) between the intended and actual droplet impact points. Specifically, the MAE was 5.56 at a wind speed of 1.5 m/s, increasing to 24.56 at 7.0 m/s, indicating the growing influence of drift at higher wind velocities. Nonetheless, the algorithm exhibits strong adaptability across different wind intensities, highlighting its robustness and accuracy. The proposed framework advances UAV spraying by enabling real-time, wind-aware corrections, thus promoting environmental sustainability, regulatory compliance, and precision agriculture. This work lays the foundation for next-generation intelligent spraying systems, with potential for future expansion through AI integration, large-scale field deployments, and performance evaluations under more complex environmental conditions.

# DSDMA: Dynamic Spray Drift Mitigation Algorithm for Optimal UAV Spraying in Agriculture

---

Rajni Goyal<sup>1\*</sup>, Srinjoy Chakraborty<sup>1</sup>, Amar Nath<sup>1</sup>, Utkarsh Niranjan<sup>1</sup>

<sup>1</sup>Sant Longowal Institute of Engineering and Technology,  
SLIET Longowal, Sangrur – 148106, Punjab, India

Emails:

- [rajni\\_pcs2103@sliet.ac.in](mailto:rajni_pcs2103@sliet.ac.in), [rajnigoyal88@gmail.com](mailto:rajnigoyal88@gmail.com)
- [c02srinjoy@gmail.com](mailto:c02srinjoy@gmail.com)
- [amarnath@sliet.ac.in](mailto:amarnath@sliet.ac.in)
- [utkarsh@sliet.ac.in](mailto:utkarsh@sliet.ac.in)

\*Corresponding Author:

Rajni Goyal

Email: [rajni\\_pcs2103@sliet.ac.in](mailto:rajni_pcs2103@sliet.ac.in)

Sant Longowal Institute of Engineering and Technology,  
SLIET Longowal, Sangrur – 148106, Punjab, India

# DSDMA: Dynamic Spray Drift Mitigation Algorithm for Optimal UAV Spraying in Agriculture

Rajni Goyal\*, Srinjoy Chakraborty, Amar Nath, Utkarsh Niranjan

*Sant Longowal Institute of Engineering and Technology, SLIET  
Longowal, Sangrur, 148106, Punjab, India*

---

## Abstract

Spray drift caused by wind remains a major challenge in UAV-based agricultural spraying, often resulting in off-target contamination, reduced application efficiency, and environmental pollution. To address this issue, this study proposes an aerodynamic-based framework to ensure precise and effective agrochemical deposition. Central to this framework is the **Dynamic Spray Drift Mitigation Algorithm (DSDMA)**, which dynamically adjusts UAV waypoints in real time by incorporating wind parameters—such as speed, direction, and flow regimes (laminar, transitional and turbulent)—to proactively correct droplet displacement before it occurs. To stabilize the UAV's trajectory under varying wind conditions, a Proportional-Integral-Derivative (PID) controller is integrated into the system. This controller effectively compensates for positional errors caused by wind-induced drag forces, ensuring improved path tracking during spraying operations. The complete framework is validated in a high-fidelity simulation environment built on AirSim, ROS2, PX4, and Unreal Engine, offering realistic aerodynamic and flight dynamics. Simulation results demonstrate that DSDMA significantly reduces spray drift, as measured by the Mean Absolute Error (MAE) between the intended and actual droplet impact points. Specifically, the MAE was 5.56 at a wind speed of 1.5 m/s, increasing to 24.56 at 7.0 m/s, indicating the growing influence of drift at higher wind velocities.

---

\*Corresponding author

Email addresses: [rajni\\_pcs2103@sliet.ac.in](mailto:rajni_pcs2103@sliet.ac.in) (Rajni Goyal),  
[c02srinjoy@gmail.com](mailto:c02srinjoy@gmail.com) (Srinjoy Chakraborty), [amarnath@sliet.ac.in](mailto:amarnath@sliet.ac.in) (Amar Nath),  
[utkarsh@sliet.ac.in](mailto:utkarsh@sliet.ac.in) (Utkarsh Niranjan)

Nonetheless, the algorithm exhibits strong adaptability across different wind intensities, highlighting its robustness and accuracy.

The proposed framework advances UAV spraying by enabling real-time, wind-aware corrections, thus promoting environmental sustainability, regulatory compliance, and precision agriculture. This work lays the foundation for next-generation intelligent spraying systems, with potential for future expansion through AI integration, large-scale field deployments, and performance evaluations under more complex environmental conditions.

*Keywords:* Precision agriculture, Wind drift, Unmanned Aerial Vehicles, Spray optimization, Spray drift, and Drone simulation.

---

## **1. Introduction**

The growing global population and economic development fuel an unprecedented demand for increased food production. Meeting this demand will require a 70% rise in agricultural yields over the next three decades (Alexandratos et al. , 2012). Agrochemicals such as pesticides and fertilizers are widely used to enhance crop productivity. However, their excessive application poses significant risks to human health and the environment. While eliminating agrochemicals entirely is impractical, optimizing their deployment through precision agriculture can mitigate these risks. Among new technologies, spray drones or Unmanned Aerial Vehicles (UAVs) are a promising option for effective and specific agrochemical spraying.

In spite of their benefits, a major challenge of wind-borne spray drift exists. It leads agrochemicals away from their desired target, as in Fig. 1. This drift lowers spraying efficiency and pollutes non-target sites, such as water bodies, neighboring crops, and ecosystems (Sánchez et al., 2023). Reducing drift is therefore necessary to provide precision, cost-effectiveness, and environmental protection in UAV-based spraying.

Spray drift is governed by a combination of controllable (operational) and uncontrollable (environmental) parameters. Controllable factors include UAV operational parameters such as nozzle type, droplet size, release height, and flight speed, while uncontrollable factors encompass environmental conditions like wind speed, temperature, and humidity (Felsot et al. , 2010). While drift cannot be completely eliminated, it can be significantly reduced through optimal UAV configurations and adaptive spraying techniques. Previous research has addressed drift reduction by manipulating controllable

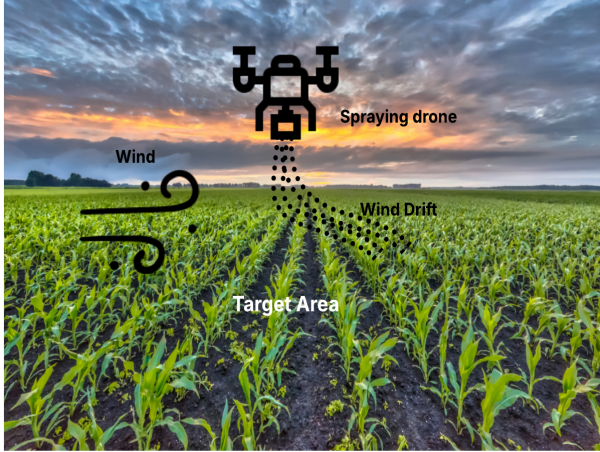


Fig. 1: Wind-induced spray drift resulting in off-target application.

parameters. As an example, (Wang et al., 2020a) tested centrifugal and hydraulic nozzles in a wind tunnel, illustrating that they have greater risks of drift with the same-sized droplets. In a parallel experiment, (Wang et al., 2020b) concluded that low droplets in high wind increase drift even at downwind distances. While these studies optimized UAV configurations (e.g., nozzle selection, flight speed), they largely ignored real-time environmental variability, limiting their field applicability.

State-of-the-art real-time spray drift mitigation solutions now incorporate dynamic UAV control algorithms that actively compensate for wind variations during operation. Faiçal et al. (Faiçal et al., 2017) developed an adaptive control system that modifies flight paths based on weather data, improving pesticide deposition. However, their approach struggles in high-wind scenarios and lacks validation in real-world farming environments. Similarly, Chen et al. (Chen et al., 2019) proposed a fuzzy logic-based system, reducing drift by 33.7% in controlled tests, but its responsiveness to sudden wind fluctuations remains inadequate.

Another study (Scagnellato, 2022) integrated aerodynamic drift models into UAV guidance systems, enhancing wind adaptability. Yet, computational inefficiencies and incomplete aerodynamic considerations hinder their scalability. Meanwhile, (An et al., 2023) explored a UAV-based methane emission suppression approach, FADE-MAS2D, for swarming drones and anomalous diffusion modeling to detect and control soil methane emissions via biochar mulch spreading. The author used aerodynamics but overlooked

49 dynamic wind-flow regimes for high wind speeds(turbulent and transitional),  
50 restricting broader implementation. While much progress has been made  
51 with UAV-based spraying and emission regulation, a number of fundamental  
52 issues still remain. Numerous current systems do not possess sufficient  
53 real-time responsiveness, being generally unable to adapt to unexpected gusts  
54 and similar sudden wind alterations. Also, computational inefficiency is an  
55 existing bottleneck because elaborate algorithms introduce delays that can  
56 affect timely decision-making. A second limitation is the overly simplified  
57 aerodynamic modeling, where transitional and turbulent wind flows are often  
58 ignored, resulting in lower accuracy in real-world applications.

59 To efficiently address the aforementioned gaps and to counteract  
60 wind-induced spray drift in UAV-based agrochemical applications, this  
61 research suggests the **Dynamic Spray Drift Mitigation Algorithm**  
62 (**DSDMA**)—a real-time adaptive control mechanism aimed at optimizing  
63 UAV flight trajectories and spraying patterns according to current wind  
64 conditions. In contrast to traditional static spraying techniques, DSDMA  
65 adapts dynamically by categorizing wind conditions into laminar, transitional,  
66 and turbulent regimes. Aerodynamic considerations are subsequently  
67 employed to calculate drag forces in each regime, while kinematic relations  
68 approximate the displacement of the drone from its desired trajectory. This  
69 categorization enables precise wind compensation, leading to uniform droplet  
70 deposition and reduced drift losses

71 Moreover, Proportional-Integral-Derivative (PID) controller (Li et al.,  
72 2006) is also incorporated within the system so that UAV tracks a specified  
73 target (e.g., position, velocity, or orientation) by constantly modifying its  
74 control inputs following the deviation between the target state and its current  
75 state. Utilizing a ROS2-AirSim-PX4 SITL simulation environment, the  
76 algorithm is thoroughly validated under various environmental conditions  
77 with high fidelity in simulating real-world agricultural spraying operations.

78 This study bridges the gap between theoretical aerodynamic modeling  
79 and practical UAV field deployment, offering a scalable and computationally  
80 efficient solution for precision agriculture. The remainder of this paper  
81 presents a detailed discussion on the algorithmic design(Section 3), simulation  
82 framework(Section 4), and performance evaluation(Section 5), demonstrating  
83 the effectiveness of DSDMA in reducing spray drift and enhancing  
84 agrochemical application accuracy.

85 **2. Material and methods**

86 *2.1. Aerodynamic Drag and Spray Dispersion*

87 Aerodynamics is the study of air interaction with the solid objects moving  
88 through it. It analysis the forces like lift, drag, thrust, and gravity influencing  
89 motion. When spraying in agricultural environments using UAVs, wind can  
90 significantly affect the trajectory of spray droplets as well as drone. The  
91 force exerted by wind causes the droplets to drift away from their intended  
92 target, reducing the effectiveness of the spraying operation. To mitigate this  
93 effect, it is essential to calculate the optimal spray position of the drone  
94 by accounting for wind speed, direction, and the resulting drag force on  
95 the droplets (Anderson, 2011). Drag force is the resistance experienced by  
96 an object moving through air. This force opposes the object's motion and  
97 limits its maximum terminal velocity. Drag can occur in laminar, turbulent,  
98 or transitional, depending on the flow conditions. In laminar flow, the air  
99 moves in smooth, parallel layers, resulting in a predictable flow pattern  
100 essential for accurate droplet placement. The drag force acting on a spherical  
101 droplet in that laminar flow regime can be calculated using Stokes' drag law  
102 equation 1 (Greenblatt and Williams, 2022; An et al., 2023).

$$f_{wl} = 6\pi\eta r \times V \quad (1)$$

103 Where:  $f_{wl}$  is the drag force for laminar,  $\eta$  is the dynamic viscosity of air,  $r$   
104 is the droplet radius, and  $V$  is the wind speed.

105 However, in turbulent flow conditions, the fluid moves chaotically and  
106 unpredictably, with swirling patterns and rapid changes in speed and direction.  
107 The wind speed is much stronger than the fluid's natural resistance (thickness  
108 or stickiness). In this case, the aerodynamic drag force acting on the moving  
109 vehicle moving through the air is calculated using Equation 2, Bagchi et al.  
110 (2003).

$$f_{wt} = \frac{1}{2} C_d \rho_{air} S V^2 \quad (2)$$

111 Where:  $f_{wt}$  denotes the drag force for turbulent flow,  $C_d$  denotes the drag  
112 coefficient,  $\rho_{air}$  represents the air density,  $S$  signifies the cross-sectional area  
113  $V$  represents the wind velocity.

114 However, when the flow is transitional, the drag force is not purely governed  
115 by Stokes' law (laminar flow) or the turbulent drag equation. Instead, it is  
116 an intermediate state where laminar and turbulent flow characteristics may

117 coexist. In this case, the drag force is typically expressed using a combination  
 118 of empirical formulas or approximations (Birouk and Abou Al-Sood, 2007).  
 119 The drag coefficient  $C_d$  is taken as a function of the Reynolds number ( $Re$ ),  
 120 interpolating between the laminar and turbulent regimes (Clift et al., 2005)  
 121 (Equation 3), and the drag force is calculated using equation 2.

$$C_d = 24 \left( \frac{1}{Re} + 0.15Re^{0.687} \right) \quad (3)$$

122 **Reynold's Number:**

123 To decide the nature of the fluid flow (laminar, transitional, and  
 124 turbulent regimes), a dimensionless and key parameter named Reynolds  
 125 number( $Re$ ) (Genç, 2012) is used. The Reynolds number is calculated using  
 126 the equation 4.

$$Re = \frac{\rho \cdot V \cdot D}{\mu} \quad (4)$$

127 Where:  $Re$  is the Reynolds number,  $\rho$  is the fluid (wind) density ( $\text{kg}/\text{m}^3$ ),  
 128  $V$  is the fluid velocity (wind velocity) ( $\text{m}/\text{s}$ ),  $D$  is the characteristic length  
 129 (diameter of the droplet or object, in meters) and  $\mu$  is the dynamic viscosity  
 130 of the fluid ( $\text{kg}/(\text{m}\cdot\text{s})$ ).

131 Table 1 shows the relation between flow type and Reynolds number.

Flow Type	Reynolds Number	Wind Speed Relationship
Laminar Flow	$Re < 2000$	Low wind speed
Transitional Flow	$2000 < Re < 4000$	Moderate wind speed
Turbulent Flow	$Re > 4000$	High wind speed

Table 1: Relationship between flow type, Reynolds number, and wind speed

132 So, by calculating the drag force depending upon the regimes, the  
 133 displacement of the spray from the target can be calculated using the kinematic  
 134 equation (Bottema and Roth, 1990).

135 *2.1.1. Mathematical framework for aerodynamic drags*

136 The drone's initial position is defined by x and y coordinates. When wind  
 137 is introduced, it alters the trajectory of the agrochemical spray, causing it to  
 138 deviate from its intended path. This deviation is measured as displacements

139  $x\_m$  and  $y\_m$  in the  $x$  and  $y$  directions, respectively. This framework  
 140 calculates the optimal drone position to ensure the spray lands accurately on  
 141 the target, compensating for the effects of aerodynamic drag.

142 To account for the effect of wind, the target positions  $x$  and  $y$  are adjusted  
 143 by adding the wind-induced displacements and changing the control law as  
 144 per Equation 5.

$$\rho(x, y, t) \rightarrow \rho(x_m, y_m, t) \quad (5)$$

145 Where,

$$x_m = x^* + V_x \quad (6)$$

$$y_m = y^* + V_y \quad (7)$$

146 Here,  $V_x$  and  $V_y$  represent the wind speed components in the horizontal  
 147 ( $x$ ) and vertical ( $y$ ) directions, respectively. The wind speed and direction  
 148 are typically measured in polar coordinates (speed and direction in degrees).  
 149 To analyze the wind's influence on the spray's trajectory, these components  
 150 are decomposed into cartesian coordinates:

$$V_x = V \cdot \cos(\theta) \quad (8)$$

$$V_y = V \cdot \sin(\theta) \quad (9)$$

152 Here,  $V$  is the wind speed, and  $\theta$  is the wind direction in radians.

153 The spray droplet's displacement due to wind during its fall is computed  
 154 by integrating the effects of wind speed and drag force over time and is  
 155 expressed by the following kinematic equations.

$$x^* = 0.5 \times (f_{w_x} \times t^{*2}) + (V_x \times t^*) + x_0 \quad (10)$$

$$y^* = 0.5 \times (f_{w_y} \times t^{*2}) + (V_y \times t^*) + y_0 \quad (11)$$

156 These equations consider the acceleration due to drag and the constant  
 157 influence of wind velocity.  $x_0$  and  $y_0$  represent the initial coordinates of the  
 158 spray target.  $t^*$  is the time it takes for a droplet to fall from a given height  $h$   
 159 to the ground under the influence of gravity and is calculated as:

$$t^* = \sqrt{\frac{2h}{g}} \quad (12)$$

160 Here,  $g$  represents the acceleration due to gravity. This time  $t^*$  is critical  
 161 to determining how long the wind will influence the trajectory of the droplet.  
 162 **Laminar flow:** The drag force is decomposed into its x and y components  
 163 according to equations 13 and 14 for laminar.

$$f_{wx} = 6\pi\eta r \times V_x \quad (13)$$

$$f_{wy} = 6\pi\eta r \times V_y \quad (14)$$

164 Where  $f_w$  is the drag force,  $\eta$  is the dynamic viscosity of air,  $r$  is the  
 165 radius of the droplet, and  $V$  is the wind speed.

166 **Turbulent flow:** For turbulent flow (high Reynolds numbers), drag force is  
 167 not linearly dependent on velocity. The drag force in turbulent conditions is  
 168 usually modeled by Equation 2. The velocity of the droplet in the direction  
 169 of the wind is updated iteratively to account for the effect of drag force. The  
 170 new velocity  $V_x(\text{new})$  is calculated as:

$$V_x(\text{new}) = V_x(\text{old}) - \frac{F_d}{m} \Delta t \quad (15)$$

171 where:  $F_d$  drag force,  $m$  mass of the droplet,  $\Delta t$  small time step for  
 172 numerical integration.

173 The total displacement of the droplet ( $x_{\text{drag}}$ ) due to wind is calculated  
 174 incrementally using the updated velocity:

$$x_{\text{drag}}+ = V_x \Delta t \quad (16)$$

175 This process is repeated for each time step, updating the droplet's velocity  
 176 based on the drag force and calculating the new displacement after each  
 177 iteration. Over time, the accumulated displacement will give the total drift  
 178 of the droplet away from the target area.

179 **Transitional flow:** This is the intermediate state, when the wind speed is  
 180 average, neither high nor low. The spray drift due to wind is calculated using  
 181 turbulent drag force. However, the drag coefficient  $C_d$  is computed using  
 182 Equation 3.

183 *2.2. Proportional-Integral-Derivative (PID) controller*

184 When wind conditions (speed and direction) remain constant during  
 185 spraying, pre-calculating the drone's optimal position based on aerodynamic

186 drag is sufficient to ensure precise spray delivery. However, in real-world  
 187 agricultural environments, wind conditions are often unpredictable, causing  
 188 fluctuations in speed and direction. Under such varying conditions,  
 189 aerodynamic drag alone cannot maintain accuracy. As a result, both the  
 190 spray droplets and the drone itself may deviate from their intended paths,  
 191 leading to ineffective spraying and potential crop damage.

192 To address this challenge, a Proportional-Integral-Derivative (PID)  
 193 controller was integrated into the droplet displacement model. The PID  
 194 controller helps mitigate positional errors caused by wind-induced drag forces,  
 195 ensuring that the drone can dynamically adjust its position in real time. It is  
 196 calculated using equation 17.

$$u[k] = K_p e[k] + K_i \sum_{i=0}^k e[i] \Delta t + K_d \frac{e[k] - e[k-1]}{\Delta t} \quad (17)$$

197 Where:  $u(t)$ : Control output at time  $t$ ,  $e(t)$ : Error, i.e., the difference  
 198 between the desired setpoint and the actual process variable,  $K_p$ : Proportional  
 199 gain,  $K_i$ : Integral gain,  $K_d$ : Derivative gain and  $\Delta t$ : Time step interval (for  
 200 discrete PID).

201 Given that significant displacement primarily occurs in transitional and  
 202 turbulent flow regimes, the PID control strategy was explicitly applied to these  
 203 cases. For computational efficiency, only the proportional term ( $K_p = 1.2$ )  
 204 was utilized for real-time corrections, while the integral ( $K_i$ ) and derivative  
 205 ( $K_d$ ) terms were set to zero. This simplification reduces processing overhead  
 206 while maintaining effective control, leading to the modified PID equation  
 207 (Equation 18).

$$u_x^{\text{prop}}(t) = K_p e_x(t). \quad (18)$$

208 The error  $e_x(t)$  is the difference between the desired position  
 209 ( $x_{\text{desired}}, y_{\text{desired}}, z_{\text{desired}}$ ) and the current position ( $x_{\text{current}}, y_{\text{current}}, z_{\text{current}}$ ) of  
 210 the drone along the three axis:

$$e_x(t) = x_{\text{desired}} - x_{\text{current}}, \quad (19)$$

$$e_y(t) = y_{\text{desired}} - y_{\text{current}}, \quad (20)$$

$$e_z(t) = z_{\text{desired}} - z_{\text{current}}. \quad (21)$$

211 The proportional term ( $K_p e(t)$ ) applies an immediate correction  
 212 proportional to the current error. If wind pushes the UAV off course, the  
 213 proportional term moves the UAV back toward the desired trajectory. The  
 214 total control signal for each axis is the sum of all three terms:

$$u_x(t) = u_x^{\text{prop}}(t) \quad (22)$$

$$u_y(t) = u_y^{\text{prop}}(t) \quad (23)$$

$$u_z(t) = u_z^{\text{prop}}(t). \quad (24)$$

215 The control outputs ( $u_x(t), u_y(t), u_z(t)$ ) are used to adjust the UAV's  
 216 position dynamically:

$$x_{\text{new}} = x_{\text{current}} + u_x(t)\Delta t, \quad (25)$$

$$y_{\text{new}} = y_{\text{current}} + u_y(t)\Delta t, \quad (26)$$

$$z_{\text{new}} = z_{\text{current}} + u_z(t)\Delta t, \quad (27)$$

217 Where  $\Delta t$  is the update time step. These adjustments ensure the UAV  
 218 maintains its desired trajectory, compensating for wind-induced drift.

219 Integrating the PID controller significantly improved the UAV's ability to  
 220 maintain its intended trajectory under varying wind conditions. The simplicity  
 221 of the proportional control mechanism ensured computational efficiency while  
 222 preserving accuracy, making it suitable for real-time agricultural operations.

### 223 3. Proposed DSDMA Algorithm

224 The proposed DSDMA (Algorithm 1) is designed to optimize the spraying  
 225 operation of a drone in agricultural environments by dynamically adjusting  
 226 its position and spraying mode based on real-time wind conditions. Initially,  
 227 the drone operates using a pre-loaded map of the target weed locations (here  
 228 assumed to be a square field with four weed locations at each corner).

229 The goal is to mitigate the impact of wind on the spray of agrochemicals,  
 230 ensuring that the target locations of the weeds receive the intended treatment  
 231 while minimizing the drift caused by the wind. The algorithm takes wind  
 232 speed  $V$  and wind direction  $\theta$  as input parameters, and other parameters  
 233 such as nozzle radius, air's dynamic viscosity, drag coefficient, gravity, and air  
 234 density are pre-defined parameters and used for drift calculations. Initially,  
 235 the drone is set to Flying state, leaving the base station to begin its spraying  
 236 operation. The spray mode is set to be Normal Spray Mode for spraying.

---

**Algorithm 1: DSDMA: Dynamic Spray Drift Mitigation Algorithm**


---

1 **Input:** Wind speed ( $V$ ) and direction ( $\theta$ ).  
 2 **Constants:** Droplet radius:  $r = 0.0002$  m, Dynamic viscosity of air:  $\eta = 1.81 \times 10^{-5}$  Pa·s, Drag coefficient (Laminar):  $C_d = 0.0679$ , Air density:  $\rho_{\text{air}} = 1.225$  kg/m<sup>3</sup>, Spray liquid density:  $\rho_{\text{fertilizer}} = 1000$  kg/m<sup>3</sup>, Acceleration due to gravity:  $g = 9.81$  m/s<sup>2</sup>, Drone speed:  $V_{\text{drone}} = 5$  m/s, Flight height:  $h = 20$  m, Flight time:  $t_{\text{flight}} = h/V_{\text{drone}}$   
 3 **Initialization:** The drone departs from its base station to commence the spraying operation.  
 4 **Drone State:** FLYING  
 5 **Spray Mode:** NORMAL  
 6 The drone navigates to the mapped weed locations and transitions its state:  
 7 **Drone State:** EXPLORATION  
 8 **if** *Drone reaches a weed location* **then**  
 9     **Drone State:** ANALYSIS The drone's sensors measure wind speed ( $V$ ) and direction ( $\theta$ ).  
       Compute the Reynolds number:

$$Re = \frac{\rho_{\text{air}} \cdot V_{\text{air}} \cdot (2r)}{\eta}$$

10     **if**  $Re < 2000$  (*Laminar Flow*) **then**  
 11         **Spray Mode:** LAMINAR Compute drift using Stokes' drag law (Eq. 1). Calculate displacement using kinematic equations (Eq. 10, Eq. 11). // The drone dynamically adjusts its position to counteract drift.  
 12         **Drone State:** SPRAYING  
 13     **else**  
 14         **if**  $2000 \leq Re < 4000$  (*Transitional Flow*) **then**  
 15             **Spray Mode:** TRANSITIONAL Compute drag coefficient  $C_d$  using Eq. 3. Calculate drag force using the drag equation (Eq. 2). Compute displacement using kinematic equations (Eq. 10, Eq. 11). **Drone State:** SPRAYING  
 16             **if** *Spraying task completed* **then**  
 17                 **Drone State:** EXPLORATION  
 18         **else**  
 19             **if**  $Re \geq 4000$  (*Turbulent Flow*) **then**  
 20                 **Spray Mode:** TURBULENT // Displacement is computed iteratively with time step  $\Delta t$ .  
 21                 Compute Reynolds number  $Re$  and drag coefficient  $C_d$ . Calculate drag force  $F_d$  using Eq. 2. Update velocity:

$$V_x(\text{new}) = V_x(\text{old}) - \frac{F_d}{m} \Delta t$$

      Compute displacement incrementally:

$$x_{\text{drag}}+ = V_x \Delta t$$

      Sum displacements over droplet fall time. **Drone State:** SPRAYING  
 22         **if** *Spraying task completed* **then**  
 23                 **Drone State:** EXPLORATION  
 24         **else**  
 25                 **Spray Mode:** EXTREME TURBULENCE // Severe wind conditions detected; abort spraying.  
 26                 **Drone State:** FLYING // The drone returns to the base station.

27 **if** *All weed locations sprayed successfully* **then**  
 28         **Drone State:** FLYING // The drone returns to its base station.  
 29 **End of Algorithm.**

237 The drone enters an **Exploration** state as it starts navigation in the  
238 field to the mapped weed locations. When it reaches a weed location, it  
239 transitions into the **Analysis** state where it measures the current wind speed  
240 and direction. Depending on the measured wind speed  $V$ , the Reynolds  
241 number is calculated. As per the RE value, the drone adjusts its spray mode  
242 as shown in Table 1, keeping the spray droplet radius at 0.0002m.

243 The drag force acting on the sprayed droplets is determined based on the  
244 prevailing flow regime, which is classified as laminar, transitional, or turbulent  
245 using the Reynolds number. Depending on the regime, the appropriate drag  
246 coefficient is applied to compute the aerodynamic resistance experienced by  
247 the droplets. Once the drag force is established, the displacement of the  
248 droplets is calculated using kinematic equations that account for factors  
249 such as wind speed, gravitational acceleration, and the initial velocity of the  
250 droplets. To mitigate spray drift, the drone dynamically adjusts its position  
251 in real-time. If the computed displacement indicates significant drift, the  
252 drone compensates by repositioning itself in the opposite direction to ensure  
253 accurate herbicide application. This adaptive correction enhances spray  
254 precision, reduces chemical wastage, and minimizes unintended exposure to  
255 non-target areas.

256 After spraying each location of the weeds, the drone checks if the task  
257 is complete. If so, it transitions back to the **FLYING** state and moves to the  
258 following weed location. Once all weed locations have been sprayed, the drone  
259 switches to **Flying Mode** and returns to its base station.

## 260 4. Environmental setup

### 261 4.1. *Simulation Environment Development*

262 The proposed wind mitigation method was tested using an integrated  
263 simulation platform developed with advanced tools including, the AirSim  
264 simulator, PX4 SITL (PX4 Development Team, 2024), Unreal Engine  
265 4, and ROS2 framework (Ma et al., 2020). All these tools collectively  
266 simulated the UAV environment, featuring high-end functionalities in terms  
267 of control, visualization, and real-world simulation. This integration ensured  
268 a seamless workflow. Fig. 2 illustrates the interactions between the different  
269 modules, including the transfer of control commands, sensor feedback, and  
270 environmental dynamics.

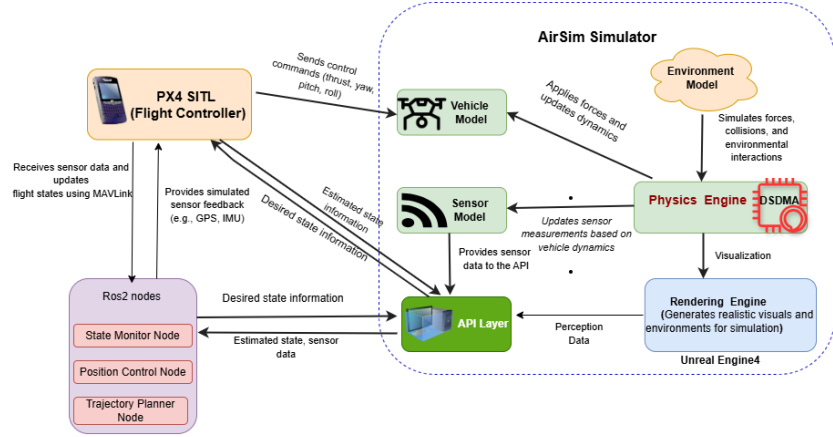


Fig. 2: Architecture of AirSim-UAV Simulation Framework Integrating PX4 SITL, Unreal Engine, and Various Models for Realistic Drone Simulation and Control

271     4.1.1. *AIRSim: Aerial Informatics and Robotics Simulation*

272     AIRSim (Microsoft Research, 2017b) is an open-source simulation  
 273     environment. It has been created by Microsoft to support realistic simulation  
 274     of autonomous vehicles, both UAVs and ground vehicles. It provides detailed  
 275     and personalized 3D environments, such as cityscapes, forests, and open spaces,  
 276     to simulate varied operational scenarios. The environment supports realistic  
 277     flight dynamics, generation of sensor data, and environmental interaction,  
 278     including wind effects, collision, and dynamic obstacles. AirSim uses an  
 279     extensible, modular architecture based on the essential components of the  
 280     environment, vehicle, physics engine, rendering engine, API layer, and sensor  
 281     models. .

282     *Components.*

283     1. **Vehicle Model:** The vehicle model is a quadrotor drone with four rotors  
 284     (Fig. 3a), intended to mimic the response of a real UAV. It includes  
 285     a variety of simulated sensors such as an Inertial Measurement Unit  
 286     (IMU) for orientation and acceleration, a barometer, GPU, cameras,  
 287     and LiDAR. The UAV can either run in manual or autonomous mode.  
 288     This research uses it in autonomous mode, which is controlled via the  
 289     AirSim API and in conjunction with PX4 flight control software and  
 290     MAVLink commands (Microsoft Research, 2017a).

291     2. **Virtual Agricultural Environment**

292 A virtual agrarian environment was created to support UAV  
 293 experimentation and verification, as illustrated in Fig. 3b. The virtual  
 294 environment simulates a natural agrarian field with crops and weeds  
 295 scattered over a flat terrain. High-resolution textures were used on the  
 296 terrain to simulate realistic soil and vegetation. This virtual environment  
 297 allows UAVs to fly over the field while inter-working with other modules.



Fig. 3: A snapshot from AirSim shows an aerial vehicle flying in an agricultural environment.

298 *4.2. Physics Engine*

299 In the physical world, UAVs are acted upon by multiple physical forces  
 300 like gravity, air density, air pressure, and magnetic fields. To correctly model  
 301 them, these physical factors are inserted into the simulation's physics engine  
 302 of AirSim(Cavalli, 2024) The proposed DSDMA algorithm was also integrated  
 303 into the simulation's physics engine for dynamic spray drift mitigation. All  
 304 parameters used to replicate real-world environmental conditions in the  
 305 simulation are as follows:

306 **1. Gravity:** In the AirSim simulation environment, gravity ( $g$ ) is typically  
 307 treated as constant with a value of  $g = 9.8 \text{ m/s}^2$ , assuming the simulation  
 308 occurs close to the Earth's surface where variations in  $g$  due to altitude  
 309 ( $h$ ) are negligible(Cavalli, 2024). However, if altitude-based variations  
 310 in  $g$  need to be accounted for, the following equation is incorporated  
 311 into the physics engine:

$$g = g_0 \cdot \frac{R_e^2}{(R_e + h)^2} \approx g_0 \cdot \left(1 - 2 \frac{h}{R_e}\right)$$

312 Where:  $g$ : gravitational acceleration at height  $h$ ,  $g_0$ : gravitational  
 313 acceleration at Earth's surface,  $R_e$ : Earth's radius,  $h$ : height above  
 314 Earth's surface.

315        2. **Air pressure and density:** In the AirSim simulation environment, air  
316        pressure and air density are not explicitly modeled by default. However,  
317        these parameters are crucial in determining the lift, drag, and propulsion  
318        forces acting on a UAV or drone. The relationship between the altitude  
319        and the pressure of the Earth’s atmosphere is complicated due to many  
320        distinct layers, each with its individual properties(Cavalli, 2024). The  
321        air density is given by:

$$\rho = \frac{P}{R \cdot T}$$

322        Where  $R$  is the specific gas constant.

#### 323        4.3. *Sensor Models*

324        AirSim has multiple sensor models for accelerometer, gyroscope, barometer,  
325        magnetometer, and GPS. We employed a gyroscope, accelerometer, and GPS  
326        in this research. The gyroscope and accelerometer are basic sensors and the  
327        core part of the Inertial Measurement Unit (IMU). The gyroscope detects  
328        the angular speed (rate of spin) of the drone about its primary axes—roll,  
329        pitch, and yaw. Accelerometer is used to measure the linear acceleration  
330        of the drone in the three axes (X,Y,Z). GPS sensor mimics the position of  
331        an autonomous aerial vehicle. Precise GPS position information is needed  
332        for navigation, mission planning, and ensuring precise movement within the  
333        simulated environment.

#### 334        4.4. *PixHawk4 Software-in-the-Loop (PX4-SITL):*

335        PX4-SITL(Microsoft, 2017) is a flight control software that manages flight  
336        motion in the simulation environment. PX4 communicates with the drone  
337        using a protocol known as MAVLink. Therefore, PX4 emulates the UAV  
338        sensors and dynamics and is a critical tool for testing flight control algorithms  
339        and software.

#### 340        4.5. *Robotic Operating System (ROS2)*

341        ROS2(Macenski et al., 2022) forms the core middleware between PX4 SITL  
342        and the simulator AirSim, enabling seamless communication and computations  
343        using its distributed node-based structure. The intended study employs several  
344        major nodes: the State Monitor Node, which monitors the UAV’s velocity,  
345        position, and drift during simulation by processing UE4 telemetry feedback;  
346        the Position Control Node, which keeps the UAV’s course by compensating  
347        for environmental disruptions such as wind; the Error Node, which senses

348 and deals with deviations, malfunctions, and sensor errors, alerting the  
349 user interface and initiating corrective measures when appropriate; and the  
350 Trajectory Planner Node, which works in tandem with the Position Control  
351 Node to compute optimal trajectories and smooth out navigation to waypoints.

## 352 5. Results and discussion

### 353 5.1. Drone Path and Initial Conditions

354 Initially, the drone was instructed to follow a few predefined waypoints,  
355 assuming the weeds' locations. These coordinates represent the drone's  
356 path at a constant altitude of -20 meters. To simulate real-world scenarios,  
357 external wind disturbances were introduced with varying speeds, directions,  
358 and flow conditions (laminar, transitional, and turbulent). These disturbances  
359 significantly affected the drone's spraying accuracy, as reflected in the drift  
360 results summarized in Table 2. The table captures six cases, each characterized  
361 by a distinct wind speed and wind direction (ranging from 30° to 70°). The  
362 wind speed range from 1.5 m/s to 7.0 m/s was chosen to reflect realistic  
363 field conditions for UAV-based agricultural spraying. Studies in precision  
364 agriculture and aerial spraying regulations suggest that UAV spraying should  
365 ideally occur within this wind speed range to maintain droplet control while  
366 ensuring operational efficiency (Volitant Technologies, 2025).

367 The original waypoints represent the UAV's planned spraying locations in  
368 wind-free conditions. However, droplet displacement necessitates adjustments  
369 to these waypoints in the presence of wind. The adjusted waypoints shift the  
370 UAV's position upwind, compensating for drift to ensure the spray reaches  
371 its intended target. The magnitude of these adjustments increases with  
372 wind speed and direction, as evident in Case 1 (1.5 m/s, 30° wind direction),  
373 where minor corrections are required, compared to Case 6 (7.0 m/s, 70° wind  
374 direction), where substantial repositioning is necessary.

375 The findings validate that DSDMA successfully reduces drift by  
376 dynamically adjusting UAV locations to offset wind influences, improving  
377 spraying accuracy. The correction method guarantees herbicides are effectively  
378 delivered on target crops, minimizing off-target contamination and enhancing  
379 overall agricultural sustainability. The results also demonstrate that  
380 integrating real-time wind compensation into UAV-based spraying systems  
381 significantly enhances operational accuracy, making DSDMA a robust solution  
382 for precision agriculture. (Volitant Technologies, 2025).

Table 2: Wind and flow characteristics with waypoint adjustments

Case	Wind Speed (m/s)	Wind Direction (°)	Droplet Radius (m)	Reynolds Number	Flow Type	Original Waypoint	Adjusted Waypoint
1	1.5	30.0	0.0002	20.30	Laminar	[30 0 -20] [30 30 -20] [0 30 -20] [0 0 -20]	[19.42 -6.11 -20] [19.42 23.89 -20] [-10.58 23.89 -20] [-10.58 -6.11 -20]
2	2.0	40.0	0.0002	27.07	Laminar	[30 0 -20] [30 30 -20] [0 30 -20] [0 0 -20]	[17.52 -10.47 -20] [17.52 19.53 -20] [-12.48 19.53 -20] [-12.48 -10.47 -20]
3	2.5	50.0	0.0002	33.84	Laminar	[30 0 -20] [30 30 -20] [0 30 -20] [0 0 -20]	[16.91 -15.60 -20] [16.91 14.40 -20] [-13.09 14.40 -20] [-13.09 -15.60 -20]
4	3.0	60.0	0.0002	40.61	Laminar	[30 0 -20] [30 30 -20] [0 30 -20] [0 0 -20]	[17.78 -21.16 -20] [17.78 8.84 -20] [-12.22 8.84 -20] [-12.22 -21.16 -20]
5	3.2	70.0	0.0002	43.31	Laminar	[30 0 -20] [30 30 -20] [0 30 -20] [0 0 -20]	[21.09 -24.49 -20] [21.09 5.51 -20] [-8.91 5.51 -20] [-8.91 -24.49 -20]
6	7.0	70.0	0.0002	94.75	Laminar	[30 0 -20] [30 30 -20] [0 30 -20] [0 0 -20]	[10.5 -53.58 -20] [10.5 -23.58 -20] [-19.5 -23.58 -20] [-19.5 -53.58 -20]

383 The proposed DSDMA algorithm is theoretically capable of adapting to  
 384 various flow regimes, including laminar, transitional, and turbulent conditions;  
 385 however, the current study focuses on laminar flow, as UAV operations  
 386 remain effective and droplet motion predictable within wind speeds up to 10  
 387 m/s. UAV operational limits and real-world agricultural spraying conditions  
 388 constrain its practical implementation. However, future work could explore  
 389 wind tunnel experiments or large-scale simulations to evaluate the algorithm's  
 390 performance in higher wind conditions, independent of UAV constraints. The  
 391 visual representation of UAV's drift under varying wind conditions is shown in  
 392 Fig.4. Each subfigure corresponds to one of the cases, illustrating the impact  
 393 of wind speed and direction on the drone's trajectory.

394 *5.2. Quantitative Validation of the DSDMA Algorithm: Mean Absolute Error  
 395 (MAE) Analysis*

396 To measure the algorithm's effectiveness quantitatively, we computed the  
 397 Mean Absolute Error (MAE) between the original target positions and the  
 398 actual spray impact locations before and after correction. The MAE is defined  
 399 as

$$\text{MAE} = \frac{1}{n} \sum_{i=1}^n |P_{\text{original},i} - P_{\text{actual},i}| \quad (28)$$

400 where:

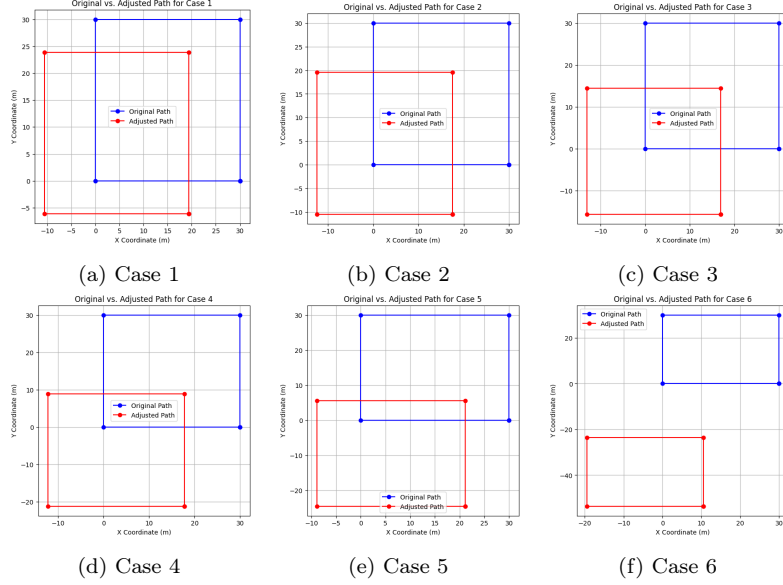


Fig. 4: Different cases of wind speed and wind direction applied

- 401 •  $n$ : Total number of waypoints or samples.
- 402 •  $P_{\text{original},i}$ : The original (target) position of the spray point.
- 403 •  $P_{\text{actual},i}$ : The actual or adjusted spray position after applying DSDMA.
- 404 The MAE values for each case, representing the deviation of the drone from  
405 its original position due to wind effects, are given in Table 3

Table 3: Mean Absolute Error (MAE) of Droplet Drift Compensation Using DSDMA

Case	Wind Speed (m/s)	MAE (m)
Case 1	1.5	5.56
Case 2	2.0	7.65
Case 3	2.5	9.56
Case 4	3.0	11.13
Case 5	3.2	11.13
Case 6	7.0	24.36

- 406 The MAE quantitatively measures the average deviation between the  
407 target spray locations (original waypoints) and the corrected UAV positions

408 (adjusted waypoints) from which spraying is performed. The algorithm's  
409 performance to counteract wind-induced drift is measured by calculating  
410 the MAE for all test cases. The lower the MAE value, the smaller the  
411 correction distance, implying the spray hits its desired target with much  
412 less deviation. On the other hand, a greater MAE indicates stronger wind  
413 conditions necessitating greater positional corrections. This linear relationship  
414 shows how effectively the DSDMA accounts for different wind conditions,  
415 enhances overall spraying efficiency, lowers herbicide loss, and lessens off-target  
416 environmental effects. The validation based on MAE thus proves DSDMA  
417 to be a scientifically sound and practically feasible solution for precision  
418 agriculture.

419

## 420 6. Conclusion

421 This study introduces an aerodynamics-inspired framework to mitigate  
422 the impact of wind on UAV spraying in precision agriculture. To achieve this,  
423 a Dynamic Spray Drift Mitigation Algorithm (DSDMA) is proposed, which  
424 dynamically adjusts the UAV's position in real time by incorporating wind  
425 speed, direction, and flow regimes into its calculations. Unlike traditional  
426 static spray methods, the algorithm guarantees the consistent delivery of  
427 droplets to their targets, enhancing deposition accuracy and improving  
428 environmental health. To further improve stability and trajectory control in  
429 spraying operations, a Proportional-Integral-Derivative (PID) controller was  
430 incorporated with DSDMA. This improved the drone's capability to sustain  
431 corrected positions in varying wind conditions with minimal deviation and  
432 strong path following.

433 The proposed system was thoroughly tested in a high-fidelity simulation  
434 environment, integrating advanced tools such as the AirSim simulator, ROS2,  
435 PX4, and Unreal Engine. The simulation setup featured an agricultural  
436 scenario with a UAV operating in realistic conditions. Results provided an  
437 optimal position of the drone to spray so that there is minimum spray drift.  
438 Mean Absolute Error (MAE), confirming the algorithm's ability to counteract  
439 drift under laminar flow conditions. While the algorithm applies to all flow  
440 regimes (laminar, turbulent, transitional), real-world UAV limitations prevent  
441 operation beyond laminar conditions, which apply to real-world agricultural  
442 spraying. In general, DSDMA improves the accuracy of agrochemical delivery  
443 and helps in sustainable agriculture by reducing off-target drift and chemical

444 excess. This research forms the basis for the future generation of smart  
445 spraying systems. Future research may investigate wind tunnel experiments  
446 or large-scale simulations to analyze the algorithm's performance under higher  
447 wind conditions, irrespective of UAV limitations. It could involve extensive  
448 field testing at large scales, algorithm tuning for challenging landscapes, and  
449 further integrating AI-supported adaptive decision-making to enhance the  
450 influence of DSDMA in practical agricultural contexts.

## 451 **Statements and Declarations**

### 452 *Competing Interests*

453 The authors declare that they have no known competing financial interests  
454 or personal relationships that could have appeared to influence the work  
455 reported in this paper.

### 456 *Author Contributions*

457 **Rajni Goyal:** Writing – original draft, Software, Methodology,  
458 Data curation. **Srinjoy Chakraborty:** Methodology, Experimentation,  
459 Conceptualization. **Amar Nath:** Writing – review & editing, Supervision,  
460 Project administration. **Utkarsh Niranjan:** Visualization, Supervision.

## 461 **References**

- 462 Alexandratos, N., & Bruinsma, J. (2012). World agriculture towards  
463 2030/2050: the 2012 revision.
- 464 Anderson, J. (2011). EBOOK: Fundamentals of Aerodynamics (SI units).  
465 McGraw hill.
- 466 An, D., Hollenbeck, D., Cao, K., & Chen, Y. (2023). Soil methane emission  
467 suppression control using unmanned aircraft vehicle swarm application of  
468 biochar mulch-A simulation study. Journal of Information and Intelligence,  
469 1(1), 68-85.
- 470 Bagchi, P., & Balachandar, S. (2003). Effect of turbulence on the drag and  
471 lift of a particle. Physics of fluids, 15(11), 3496-3513.

- 472 Bennetts, V. H., Kucner, T. P., Schaffernicht, E., Neumann, P. P., Fan, H.,  
473 & Lilienthal, A. J. (2017). Probabilistic air flow modelling using turbulent  
474 and laminar characteristics for ground and aerial robots. *IEEE robotics*  
475 and automation letters
- 476 Birouk, M., & Abou Al-Sood, M. M. (2007). Numerical study of sphere  
477 drag coefficient in turbulent flow at low Reynolds number. *Numerical Heat*  
478 *Transfer, Part A: Applications*, 51(1), 39-57.
- 479 Bottema, O., & Roth, B. (1990). *Theoretical kinematics* (Vol. 24). Courier  
480 Corporation.
- 481 Boychev, I. Z. (2018, September). Research algorithms to optimize the  
482 drone route used for security. In *2018 IEEE XXVII International Scientific*  
483 *Conference Electronics-ET* (pp. 1-4). IEEE.
- 484 Cavalli, A. (2024). Development of a simulation environment for precision  
485 agriculture applications with Unmanned Aircraft Systems (Doctoral  
486 dissertation, Politecnico di Torino).
- 487 Chen, Y., Hou, C., Tang, Y., Zhuang, J., Lin, J., & Luo, S. (2019). An effective  
488 spray drift-reducing method for a plant-protection unmanned aerial vehicle.  
489 *International Journal of Agricultural and Biological Engineering*, 12(5),  
490 14-20.
- 491 Chen, S., Lan, Y., Zhou, Z., Ouyang, F., Wang, G., Huang, X., ... & Cheng,  
492 S. (2020). Effect of droplet size parameters on droplet deposition and drift  
493 of aerial spraying by using plant protection UAV. *Agronomy*, 10(2), 195.
- 494 Chen, S., Lan, Y., Zhou, Z., Deng, X., & Wang, J. (2021). Research advances  
495 of the drift reducing technologies in application of agricultural aviation  
496 spraying. *International Journal of Agricultural and Biological Engineering*,  
497 14(5), 1-10.
- 498 Chowdhury, S., Shahvari, O., Marufuzzaman, M., Li, X., & Bian, L. (2021).  
499 Drone routing and optimization for post-disaster inspection. *Computers &*  
500 *Industrial Engineering*, 159, 107495.
- 501 Clift, R., Grace, J. R., & Weber, M. E. (2005). *Bubbles, drops, and particles*.

- 502 Dorling, K., Heinrichs, J., Messier, G. G., & Magierowski, S. (2016). Vehicle  
503 routing problems for drone delivery. *IEEE Transactions on Systems, Man,  
504 and Cybernetics: Systems*, 47(1), 70-85.
- 505 Faiçal, B. S., Pessin, G., Filho, G. P., Carvalho, A. C., Gomes, P. H., &  
506 Ueyama, J. (2016). Fine-tuning of UAV control rules for spraying pesticides  
507 on crop fields: An approach for dynamic environments. *International  
508 Journal on Artificial Intelligence Tools*, 25(01), 1660003.
- 509 Faiçal, B. S., Freitas, H., Gomes, P. H., Mano, L. Y., Pessin, G., de Carvalho,  
510 A. C., ... & Ueyama, J. (2017). An adaptive approach for UAV-based  
511 pesticide spraying in dynamic environments. *Computers and Electronics in  
512 Agriculture*, 138, 210-223.
- 513 Felsot, A. S., Unsworth, J. B., Linders, J. B., Roberts, G., Rautman, D.,  
514 Harris, C., & Carazo, E. (2010). Agrochemical spray drift; assessment and  
515 mitigation—A review. *Journal of Environmental Science and Health Part  
516 B*, 46(1), 1-23.
- 517 Ferguson, J. C., O'Donnell, C. C., Chauhan, B. S., Adkins, S. W., Kruger, G.  
518 R., Wang, R., ... & Hewitt, A. J. (2015). Determining the uniformity and  
519 consistency of droplet size across spray drift reducing nozzles in a wind  
520 tunnel. *Crop Protection*, 76, 1-6.
- 521 Genç, M. S. (Ed.). (2012). Low Reynolds Number: Aerodynamics and  
522 Transition. BoD—Books on Demand.
- 523 Greenblatt, D., & Williams, D. R. (2022). Flow control for unmanned air  
524 vehicles. *Annual Review of Fluid Mechanics*, 54(1), 383-412.
- 525 Johnson, M. A., & Moradi, M. H. (2005). PID control (pp. 47-107). London,  
526 UK: Springer-Verlag London Limited.
- 527 Kethineni, K. K., Mohanty, S. P., Kougianos, E., Bhowmick, S., & Rachakonda,  
528 L. (2024). SprayCraft: Graph-Based Route Optimization for Variable Rate  
529 Precision Spraying. *arXiv preprint arXiv:2412.12176*.
- 530 Li, Y., Ang, K. H., & Chong, G. C. (2006). PID control system analysis and  
531 design. *IEEE Control Systems Magazine*, 26(1), 32-41.

- 532 Liu, Q., Shan, C., Zhang, H., Song, C., & Lan, Y. (2023). Evaluation of liquid  
533 atomization and spray drift reduction of hydraulic nozzles with four spray  
534 adjuvant solutions. *Agriculture*, 13(2), 236.
- 535 Macenski, S., Foote, T., Gerkey, B., Lalancette, C., & Woodall, W. (2022).  
536 Robot operating system 2: Design, architecture, and uses in the wild.  
537 *Science robotics*, 7(66), eabm6074.
- 538 Ma, C., Zhou, Y., & Li, Z. (2020, April). A new simulation environment  
539 based on AirSim, ROS, and PX4 for quadcopter aircrafts. In 2020 6th  
540 international conference on control, automation and robotics (ICCAR) (pp.  
541 486-490). IEEE.
- 542 Marubayashi, R. Y., Oliveira, R. B. D., Ferreira, M. D. C., Roggia, S.,  
543 Moraes, E. D. D., & Saab, O. J. (2021). Insecticide spray drift reduction  
544 with different adjuvants and spray nozzles. *Revista Brasileira de Engenharia  
545 Agrícola e Ambiental*, 25, 282-287.
- 546 Microsoft, “PX4 SITL integration,” [Online]. Available:  
547 [https://microsoft.github.io/AirSim/px4\\_sitl/](https://microsoft.github.io/AirSim/px4_sitl/).
- 548 Microsoft Research, “Vehicle selection API,” 2017. [Online]. Available:  
549 <https://microsoft.github.io/AirSim/apis/>.
- 550 Microsoft Research, “AirSim: A simulation platform for AI research and  
551 experimentation,” [Online]. Available: <https://microsoft.github.io/AirSim/>.  
552 [Accessed: Dec. 31, 2024].
- 553 PX4 Development Team, “Gazebo Simulation PX4  
554 v1.9.0 Developer Guide,” [Online]. Available:  
555 [https://dev.px4.io/v1.9.0\\_noredirect/en/simulation/gazebo.html](https://dev.px4.io/v1.9.0_noredirect/en/simulation/gazebo.html).  
556 [Accessed: Dec. 31, 2024].
- 557 Scagnellato, L. (2022). Multi-rotor UAS for precision crop-spraying:  
558 developing an adaptive guidance algorithm to minimize spray drift in  
559 a wind environment (Doctoral dissertation, Politecnico di Torino).
- 560 Sánchez-Fernández, L., Barrera, M., Martínez-Guanter, J., & Pérez-Ruiz, M.  
561 (2023). Drift reduction in orchards through the use of an autonomous UAV  
562 system. *Computers and Electronics in Agriculture*, 211, 107981.

- 563 Shyy, W., Lian, Y., Tang, J., Viieru, D., & Liu, H. (2008). Aerodynamics of  
564 low Reynolds number flyers.
- 565 Srivastava, K., Pandey, P. C., & Sharma, J. K. (2020). An approach for route  
566 optimization in applications of precision agriculture using UAVs. *Drones*,  
567 4(3), 58.
- 568 Volitant Technologies. (2025). Agras T40 quick specs. Retrieved April 11,  
569 2025, from <https://volitantdrones.com/agras-t40-quick-specs/>
- 570 Wang, C., Zeng, A., He, X., Song, J., Andreas, H., & Gao, W. (2020). Spray  
571 drift characteristics test of unmanned aerial vehicle spray unit under wind  
572 tunnel conditions. *International Journal of Agricultural and Biological  
573 Engineering*, 13(3), 13-21.
- 574 Wang, G., Han, Y., Li, X., Andaloro, J., Chen, P., Hoffmann, W. C., ... &  
575 Lan, Y. (2020). Field evaluation of spray drift and environmental impact  
576 using an agricultural unmanned aerial vehicle (UAV) sprayer. *Science of  
577 the Total Environment*, 737, 139793.

**Declaration of interests**

The authors declare that they have no known competing financial interests or personal relationships that could have appeared to influence the work reported in this paper.

The authors declare the following financial interests/personal relationships which may be considered as potential competing interests:



Click here to access/download  
**LaTeX Source Files**  
changelog.txt



Click here to access/download  
**LaTeX Source Files**  
elsarticle-harv.bst



Click here to access/download  
**LaTeX Source Files**  
elsarticle-num-names bst



Click here to access/download  
**LaTeX Source Files**  
elsarticle-num.bst



Click here to access/download  
**LaTeX Source Files**  
`elsarticle-template-harv.tex`





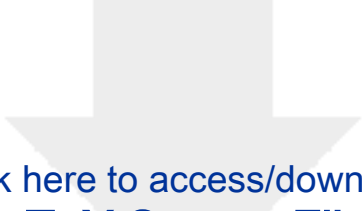
Click here to access/download  
**LaTeX Source Files**  
`elsarticle-template-num-names.tex`



Click here to access/download  
**LaTeX Source Files**  
elsarticle.dtx



Click here to access/download  
**LaTeX Source Files**  
`elsarticle.ins`



Click here to access/download  
**LaTeX Source Files**  
**README**





Click here to access/download  
**LaTeX Source Files**  
manifest.txt